(Presented at XIVth International Conference on
High Energy Physics, August 28 - September 5, 1968,
Vienna, Austria)

SLAC-PUB-532
(EXP)

PHOTOPRODUCTION OF RHO MESONS AT 9 BeV

by

F. Bulos, W. Busza, R. Diebold, R. Giese,
R. R. Larsen, D. W. G. S. Leith, B. Richter and R. Russell

Stanford Linear Accelerator Center
Stanford University, Stanford, California

L. Kauffman, V. Perez-Mendez, A. Stetz and S. H. Williams

Lawrence Radiation Laboratory
University of California, Berkeley, California

and

M. Beniston and J. Rettberg

IBM Scientific Center, Palo Alto, California

I. Introduction

We wish to present preliminary results of a study of vector meson production by 9 BeV monochromatic photons. These results are the first part of a systematic survey of vector meson photoproduction from 5 BeV to 18 BeV, using a large acceptance wire spark chamber spectrometer. The experiments from 5 BeV through 9 BeV have been performed with the partially monochromatic annihilation photon beam, while the data above 9 BeV have been performed with a conventional zero degree Bremsstrahlung photon beam. The wire spark chamber spectrometer is on-line to an

---

Work performed under the auspices of the U. S. Atomic Energy Commission

1800 computer which logs our raw data onto magnetic tape, does a full kinematical analysis of the events as they come in, and updates histograms which are displayed on a memory scope and performs monitoring operations on most of our experimental equipment. The experiment has been performed on six complex nucleii targets, (berylium, carbon, aluminum, copper, silver and lead), and with liquid hydrogen and deuterium targets. However, only the 9 BeV data will be presented here and it should be emphasized that the analysis of this data is very preliminary.

II. Photon Beam

A high energy monochromatic photon beam, which utilizes the annihilation radiation from positrons in flight, was used for this experiment. Positrons of about 12 BeV produced by the SLAC two-mile accelerator, were momentum analyzed in the beam switchyard to $\pm$ .5% and directed onto a small hydrogen target 30 cm long. Collimators were used to define the photon production angle of around 6 mrad to high precision. The small angle intense bremsstrahlung from the hydrogen target are absorbed in these collimators and some primary shielding just upstream of them. Three large (30 kg meter) sweeping magnets clean the beam of all charged products produced down the beam line. The transmitted photon beam has an energy spectrum consisting of a monochromatic peak resulting from the two-body final state of annihilation, superimposed upon a large angle bremsstrahlung spectrum of roughly equal magnitude.

This beam passed through 2/3 radiation length of lithium hydride hardener to remove very low energy γ's.

The resolution of the monochromatic peak under our experimental conditions was $\sim \pm 1.5\%$ and gave some 300 monochromatic photons per pulse at 300 pulse per second operation of the linac. The beam size at our target, 30 meters away from the liquid hydrogen production target, was six inches high by one-half inch wide, and the effective production angle for the 9 BeV configuration was of the order of 4 mrads. The bremsstrahlung background underneath the monochromatic peak region was found to be less than 5%. The energy spectrum of the photon beam was measured from time to time throughout the experiment by using the wire chamber spectrometer as an electron-positron pair spectrometer. The typical energy distribution is shown in Fig. 1. The low energy cutoff comes from the geometrical cutoff of the wire spark chambers. The curve has not been corrected for the inherent resolution of the spectrometer system.

III. Apparatus

The meson spectrometer consists of a wide aperture, uniform field magnet, followed by a set of trigger counters and four wire spark chambers, with magnetostrictive readout, interfaced to an on-line IBM 1800 computer. A schematic layout of the apparatus is shown in Fig. 2. The photon beam is collimated and swept free of charged particles and then passes through the meson production target before burying itself in a 40 cm tungsten beam stopper. The beam stopper was 10 cm wide, and filled the gap of our

window frame spectrometer magnet with 100 x 40 cm aperture and 30 kg meters field. The photo-produced meson decaying rapidly into π mesons, which then passed through the magnet aperture into detection region. Eight large-area scintillation counters made up the trigger system. The last counters were paired together and demanded a coincidence and the overall trigger was signalled by any five out of six counter combinations firing within a 15 nanosecond coincidence gate. When two or more particles passed through this system and satisfied the trigger requirement the high voltage was applied to the wire spark chambers, the total delay time from the passage of particles to application of the high voltage to the chambers was about 420 nanoseconds.

The wire spark chamber system consisted of four wire spark chambers behind the magnet and one spark chamber mounted at the center of the spectrometer magnet. Each of the four outside chambers consisted of four planes, each with wire strung respectively at 0°, 30°, 60° and 90° to vertical. The size of these chambers varied between 120 x 43 cm for the front chambers, to 150 x 75 cm for the back chambers. The wire spacing was 1 mm in all chambers. The magnet chamber was constructed to give information on the lateral position only and was used to find the point of origin of interaction when the experiment utilized the long liquid hydrogen/deuterium target.

The spark chamber information was read out on 17 magnetostrictive wands; one for the magnet chamber and four for each wire plane in each of the four back chambers. The read out electronics consisted of 16 channels of four 13-bit scalers each, and an additional channel (for

the magnet chamber) of eight 13-bit scalers. These scalers are started by the first fiducial pulse from the wand and count down from a 20 megacycle per cycle clock. Each scaler in a channel is stopped by the successive pulses giving a maximum of four coordinates per plane (except for the magnet chamber which has eight scalers). These scalers are then read into the 1800 computer one by one via a single 16 bit digital input. The trigger counter information and the status of 32-counter hodoscope is also read into the 1800 on another digital input for each event.

The spectrometer system records data at about six events per second and under these circumstances completely analyses all events.

The spectrometer has an acceptance of about 1000 MeV in mass at any given acceptance with a maximum detectable mass of the order of 3500 MeV. The mass resolution varies from about $\pm$ 8 MeV at 700 MeV to about $\pm$ 18 MeV at about 3000 MeV mass. The momentum transfer acceptance goes from 0 to about 0.25 $(\text{GeV/c})^2$ with a momentum transfer resolution of the order of 0.0001 $(\text{GeV/c})^2$. The apparatus accepts about 80% of the decay angular distribution of the produced meson states.

The information from the spectrometer is logged on tape for each event and then, time permitting, a complete kinematic analysis is performed on the event and the various interesting physical quantities is calculated and histogrammed. The on-line system also enables a constant monitor to be kept on the counter and spark chamber efficiencies, the settings of our magnets, collimators, targets, and counters, and the intermediate status of the scaler bank.

A more complete description of the hardware and software is published elsewhere.

IV. Discussion of the data, and analysis

The data presented here comes from a three-week run of the wire spark chamber spectrometer in the monochromatic photon beam. Data were taken at the three energies, 5, 7, and 9 BeV, with six complex nucleon targets and with hydrogen and deuterium targets. Thickness of the target material varied from 0.1 radiation lengths for beryllium target up to 0.3 radiation lengths for the lead target, while the liquid hydrogen/deuterium target was 1 meter long. Comparable amounts of data were collected at each energy and the final number of ρ's within our $\pm$ 3% energy cut varied from about 1000 for the low z materials where the data rates were reasonably high, down to some 300 events for the high z materials, where the data rates were considerably slower. The hydrogen/deuterium samples are somewhat larger - being the order of 5000 for each liquid at each energy.

The mass spectra for each of our six targets for 9 BeV photon energy are shown in Fig. 3a. The events are plotted in 50 MeV bins and the contents of these bins are corrected for the acceptance of the spectrometer. In Fig. 3b the mass distribution for beryllium is shown separately, in bins of 20 MeV. The peak of the mass distribution appears for each element around 750 to 760 MeV and the high mass rapid fall characteristic of this process is still clearly present.

No systematic fitting to these mass spectra have yet been done, however, the data is consistent with a mass of 765 MeV and a width of 120 MeV as is shown in Fig. 4a and 4b for the beryllium and carbon data. The curve represents a standard Breit-Wigner superimposed on a coherent background of diffraction pion exchange as described by Soding. We have made no investigations of the necessity of the $(M_\rho/M_{\pi\pi})^4$ factor required by Ross-Stodolsky theory.

The momentum transfer distribution for each of the six target materials is shown in Fig. 5. The contents of the bins are again events corrected for the acceptance of the spectrometer and typical bin size is equal to .0002 $(\text{GeV/c})^2$. The plots show the characteristic steep diffraction slope observed at low energies and the rapid change of slope between beryllium and lead characteristic of the form factor of the complex target nucleus. These distributions have been fitted with a form

$$\frac{d\sigma}{dt} = Ae^{-Bt} + Ce^{-8t}$$

A summary of these fits is shown in Table I, and the forward cross section and exponential slope corrected for our acceptance, decays in flight, photon flux, etc., are shown in Table II. The data show the characteristic marked increase in diffraction slope as observed by others. In Table III we compare the measurements of the diffraction slope with those of pp scattering at 20 BeV of Belletini et al. and with the two ρ meson photoproduction experiments from DESY, Asbury et al., and Blechschmidt et al. The forward cross section for the ρ photoproduction process is compared with the two DESY experiments in Table IV. The agreement between the three experiments for those elements which measured in common is satisfactory except for the lead point.

In Fig. 6 the forward cross section per nucleon relative to that of copper is plotted against the atomic number of the target material. This method is supposed to allow determination of the total ρ-nucleon cross section. We show a curve for the A-dependence if the total ρ nucleon cross section were 40 mb, our data is entirely consistent with such a value; however, the data is equally consistent if the curve is drawn for ρ nucleon total cross sections of 20 and 30 mb. It is clear that our data at present is not able to extract an accurate value for this total cross section.

From the vector dominance model we can derive the relation between the forward differential cross section for photo ρ production, the coupling constant for for the photon to the ρ and the total ρ-nucleus cross section. Taking the measured proton nucleus cross sections from Belletini et al., and assuming that they are approximately equal to the total ρ nucleus cross section, we have calculated a value for the photon rho coupling constant, $\gamma_\rho^2/4\pi$, for each target material. The results are shown in Fig. 7. It must be emphasized that the analysis at 9 BeV is extremely preliminary and especially so for the absolute calculation of the coupling constant. The errors are very large and are mainly due to the substantial corrections we had to make to our data which amount to about a factor of 2 in each case. These corrections have not yet been sufficiently studied and the estimated systematic error to the corrections dominates the error of our forward cross sections and also of the calculation of the coupling constant. Therefore , we will be able to reduce this error by about a factor of 2-3 during the next few months. In addition we have a substantial amount of data at 5 BeV and 7 BeV of the same reactions being analysed at present. It is therefore hoped we will be able to make a more

definate and conclusive determination of this coupling constant within the next few months. The mean value for determination of the photon-ρ coupling constant is $1.2 \pm .3$. The forward cross section per nucleon and our calculated value of the coupling constant for each target material are shown in Table V.

V. Conclusions

The photo production of rho mesons at 9 BeV remains a dominant reaction in the γ to 2π channel as previously observed at lower energies. The ρ meson continues to have asymmetric shape which is now characteristic of photoproduction and preliminary fits to our data indicate that it is consistent with a mass of about 765 and a width of about 120 MeV. However, no systematic work has been done on determining the best shape of the rho from our experiment. The differential cross sections show the characteristic diffraction-like behaviour and our slopes agree very well with those published for the proton scattering experiments at 20 BeV. The determination of the ρ-nucleus total cross section from our experiment is not very sensitive but is consistent with the value of 30-40 mb. Finally, an estimate of the coupling constant between the photon and the ρ meson has been made under the assumptions of the vector dominance model obtaining a mean value of $\frac{\gamma_\rho^2}{4\pi} = 1.2 \pm 0.3$.

SUMMARY OF FITS TO

MOMENTUM TRANSFER DISTRIBUTIONS

Material	A	B	C	χ^2	Number of data points
Beryllium	236	-56	14.8	108	68
Carbon	139	-73	3.6	38.7	35
Aluminum	265	-99	0.5	29.1	33
Copper	419	-158	3.3	23	26
Silver	277	-244	1.5	9.3	14
Lead	530	-342	2.5	14.2	20

(These numbers are from fits to raw data and are not corrected for photon flux, etc.)

TABLE I

DIFFERENTIAL CROSS SECTION PARAMETERS

FOR $\gamma A \rightarrow pA$ at 9 BeV

Material	A ($\mu b/GeV^2$ nuclear)	B $(GeV/c)^{-2}$
Beryllium	470 ± 100	56 ± 10
Carbon	700 ± 180	73 ± 10
Aluminum	1140 ± 300	99 ± 10
Copper	2260 ± 600	158 ± 15
Silver	3520 ± 950	244 ± 20
Lead	3420 ± 900	342 ± 20

$$\frac{d\sigma}{dt} = Ae^{-Bt} + Ce^{-8t}$$

TABLE II

COMPARISON OF DIFFRACTION SLOPES, B.

$$\frac{d\sigma}{dt} = A_e^{-Bt} + C_e^{-8t}$$

Material		B $(GeV/c)^{-2}$		
	pA*	γA (DESY-I)/	γA (DESY-II)x	γA (SLAC)
Beryllium	77	-		56 ± 10
Carbon	67	47 ± 3	48 ± 5	73 ± 10
Aluminum	111	-	73 ± 9	99 ± 10
Copper	200	139 ± 7		158 ± 15
Silver				244 ± 20
Lead	362	290 ± 12		342 ± 20

* 20 BeV/c pA → pA Belletini, et al.

/ J. G. Asbury et al. Phys. Rev. Letters 19, 865 (1967).

x H. Blechschmidt et al., Proceedings Stanford Conf. (1967).

TABLE III

COMPARISON OF FORWARD CROSS SECTIONS, A

$$\frac{d\sigma}{dt} = Ae^{-Bt} + Ce^{-8t}$$

$$\left(\frac{d\sigma}{dt}\right)_{t=0} = A \ (\mu b/GeV^2 \text{ nucleon})$$

Material	A (μb/GeV^2 nucleon)		
	DESY I[1]	DESY II[2]	SLAC
Beryllium	-	-	470 ± 100
Carbon	800 ± 64	683 ± 96	700 ± 180
Aluminum		1170 ± 420	1140 ± 300
Copper	1790 ± 170		2260 ± 600
Silver			3520 ± 950
Lead	1600 ± 160		3420 ± 900

[1] J. G. Asbury et al., Phys. Rev. Letters 19, 865 (1967).

[2] H. Blechschmidt et al., Proceedings Stanford Conference (1967).

TABLE IV

Material	$\frac{1}{A}\left(\frac{d\sigma}{dt}\right)_{t=0}$	$\frac{\gamma\rho^2}{4\pi}$
Beryllium	470	$1.7 \pm .46$
Carbon	700	$1.25 \pm .34$
Aluminum	1140	$1.43 \pm .39$
Copper	2260	$1.19 \pm .32$
Silver	3520	$1.08 \pm .29$
Lead	3420	$1.47 \pm .4$

Mean Value of Coupling Constant

$$\frac{\gamma\rho^2}{4\pi} \sim 1.2 \pm .3$$

TABLE V

Figure Captions

Fig. 1a — Energy spectrum of the beam as measured in the pair spectrometer mode.

$$\gamma\ Al \rightarrow e^+e^-\ Al$$

Fig. 1b — Energy spectrum of the beam, as measured from the rho momentum distribution.

$$\gamma\ Be \rightarrow \pi^+\pi^-Be.$$

Fig. 2 — Schematic drawing of the spectrometer.

Fig. 3a — Two pion mass spectra for 9 BeV photons incident on Be, C, Al, Cu, Ag and Pb targets. The contents of the histograms have been corrected for the acceptance of the system.

Fig. 3b — A higher resolution plot of the two-pion mass spectrum for Be target.

Fig. 4a,b — The two pion mass spectrum for 9 BeV photons incident on (a) Be target, and (b) carbon target. The solid curve represents a normal Breit-Wigner for the rho, interfering with a pion diffraction scattering amplitude, as described by Soding.

Fig. 5 — The momentum transfer distribution for 9 BeV photoproduction of rho mesons from Be, C, Al, Cu, Ag and Pb. The data has been corrected for the acceptance of the system.

Fig. 6 — The relative forward cross section per nucleon as a function of the atomic number of the material. The solid line represents the behaviour expected for a total ρN cross-section of 40 mb.

Fig. 7 — The calculated value for the rho-photon coupling constant, $\gamma_\rho^2/4\pi$, is shown as a function of the atomic number.

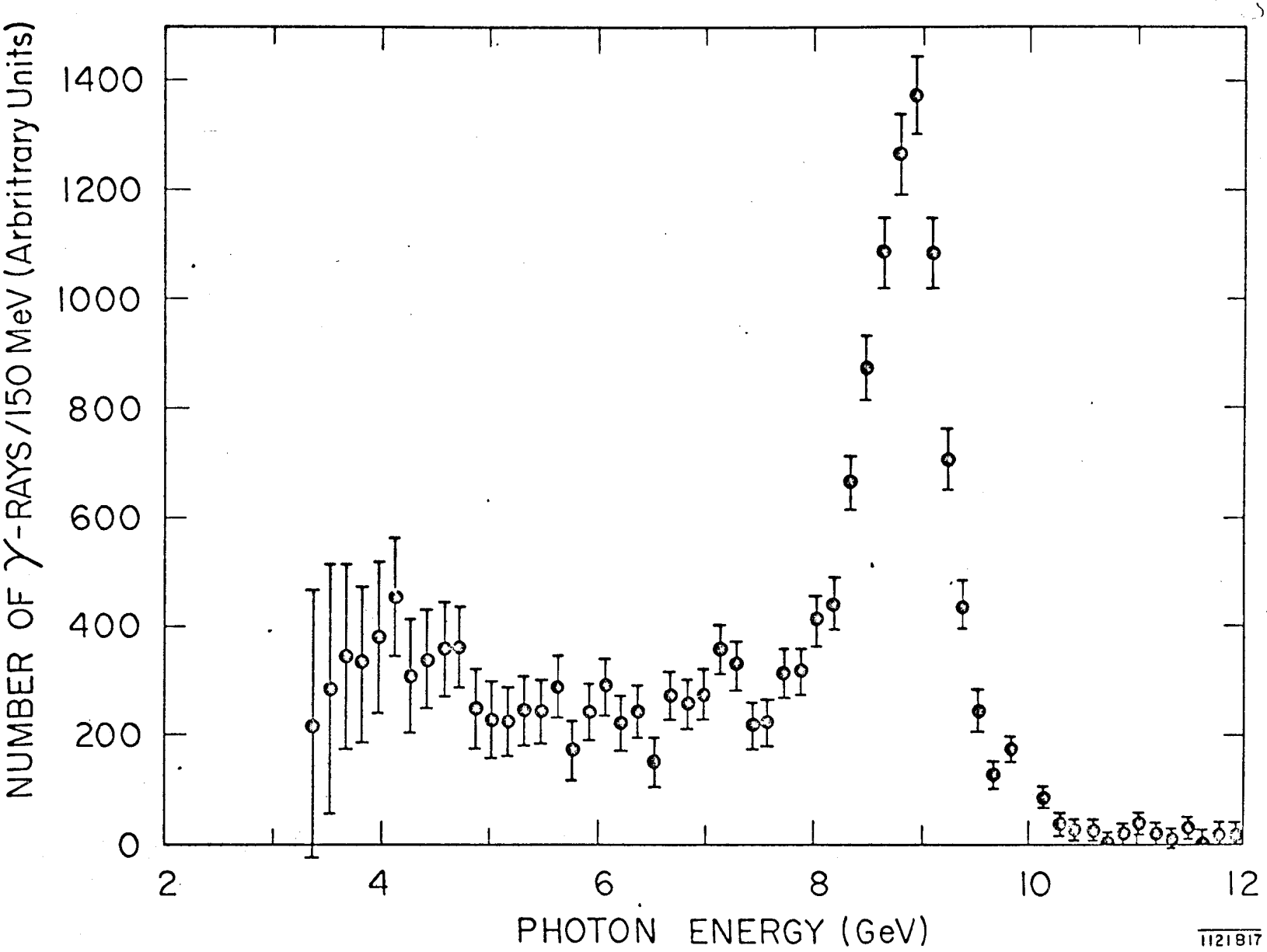
NUMBER OF γ-RAYS/150 MeV (Arbitrary Units)
0
200
400
600
800
1000
1200
1400
2
4
6
8
10
12
PHOTON ENERGY (GeV)
1121817

Fig.1a

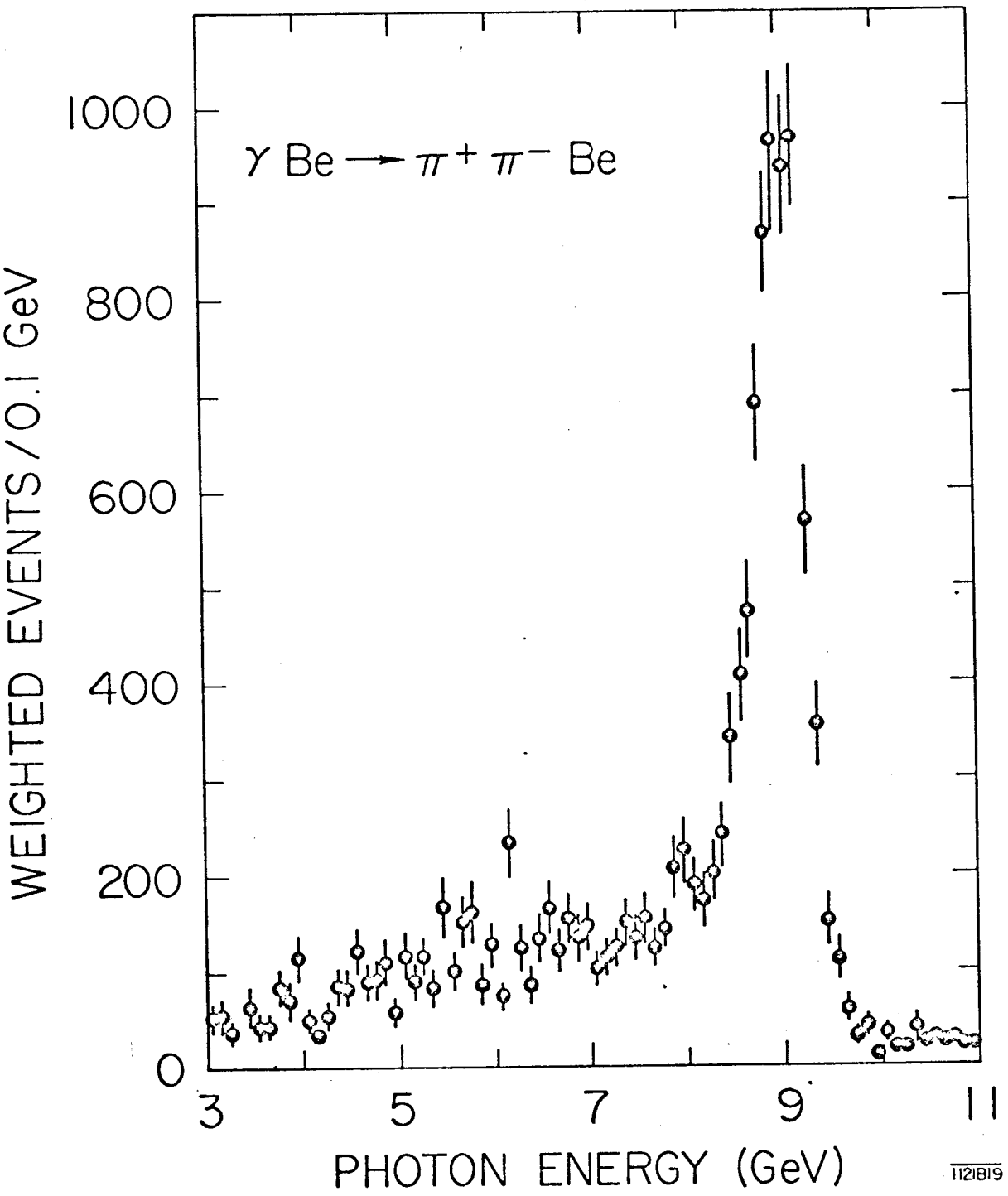
γ Be $\rightarrow \pi^+ \pi^-$ Be
WEIGHTED EVENTS / 0.1 GeV
1000
800
600
400
200
0
3
5
7
9
11
PHOTON ENERGY (GeV)
112819

Fig.1b

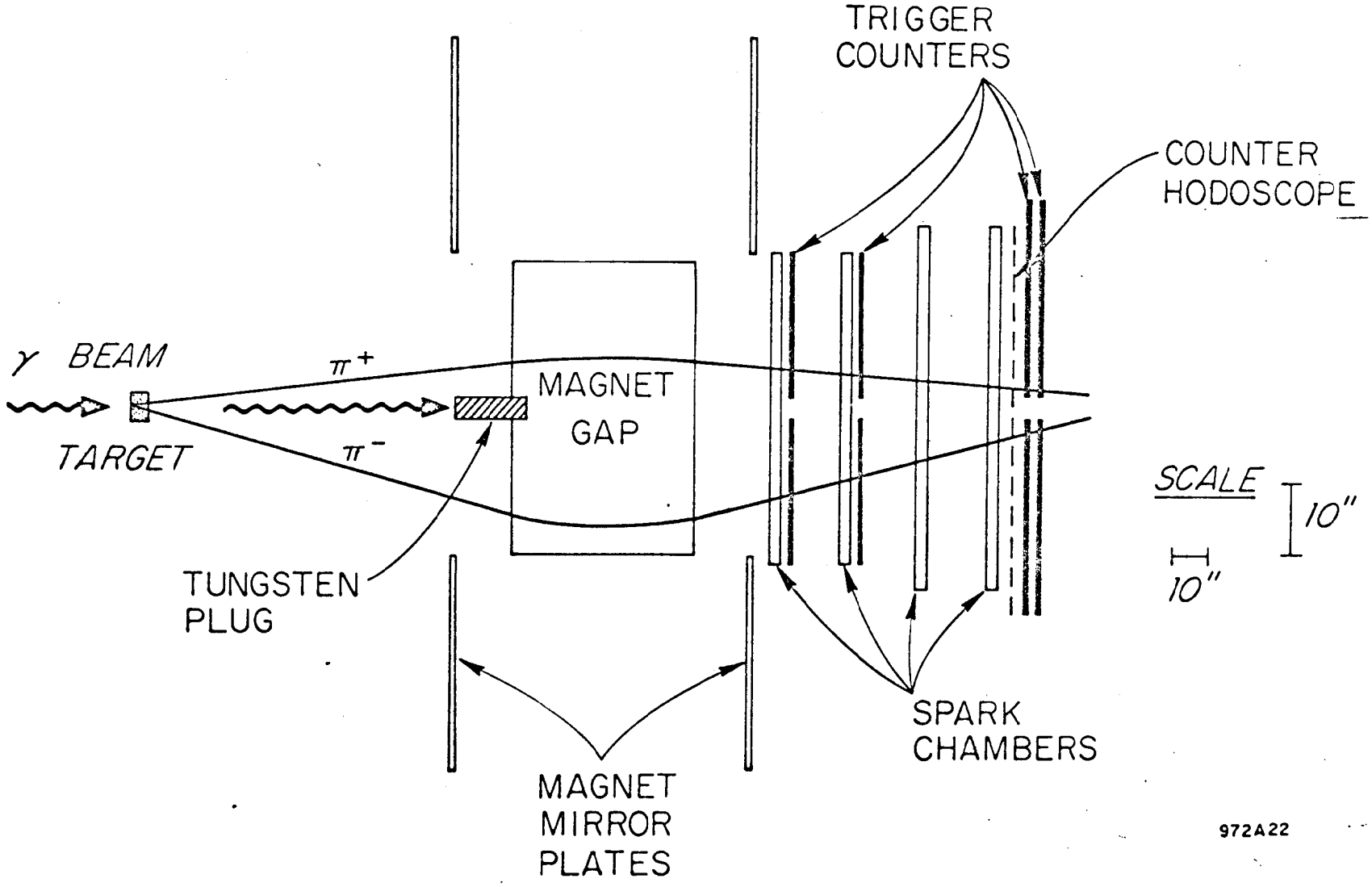
TRIGGER
COUNTERS
COUNTER
HODOSCOPE
γ BEAM
π+
MAGNET
GAP
TARGET
π−
SCALE
10"
10"
TUNGSTEN
PLUG
SPARK
CHAMBERS
MAGNET
MIRROR
PLATES
972A22

Fig.2

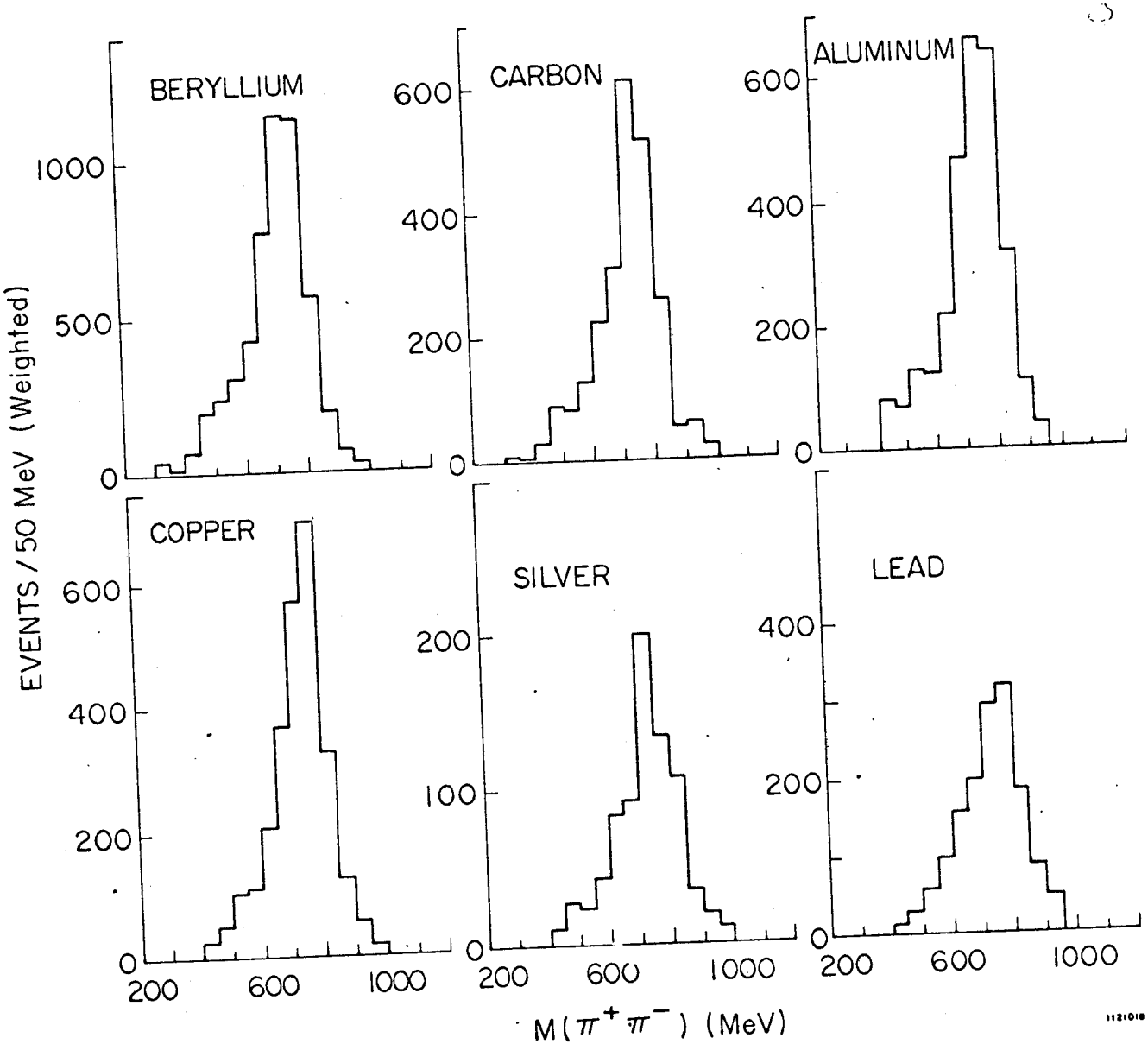
BERYLLIUM
CARBON
ALUMINUM
COPPER
SILVER
LEAD
EVENTS / 50 MeV (Weighted)
M(π⁺π⁻) (MeV)
0
200
400
500
600
1000
100
600
1000
112:018

Fig.3a

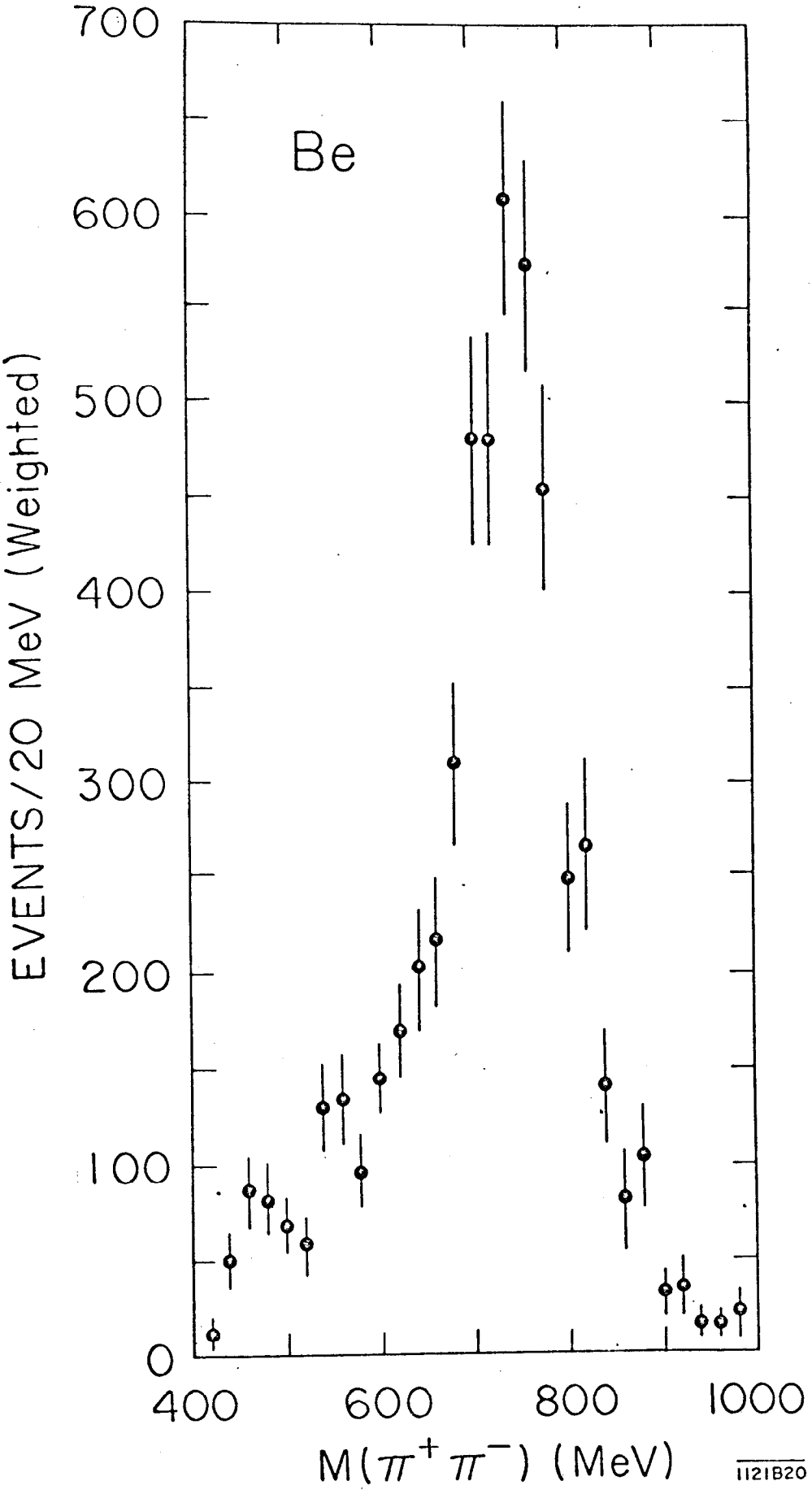
Be
EVENTS/20 MeV (Weighted)
700
600
500
400
300
200
100
0
400
600
800
1000
M(π⁺π⁻) (MeV)
1121B20

Fig. 3b

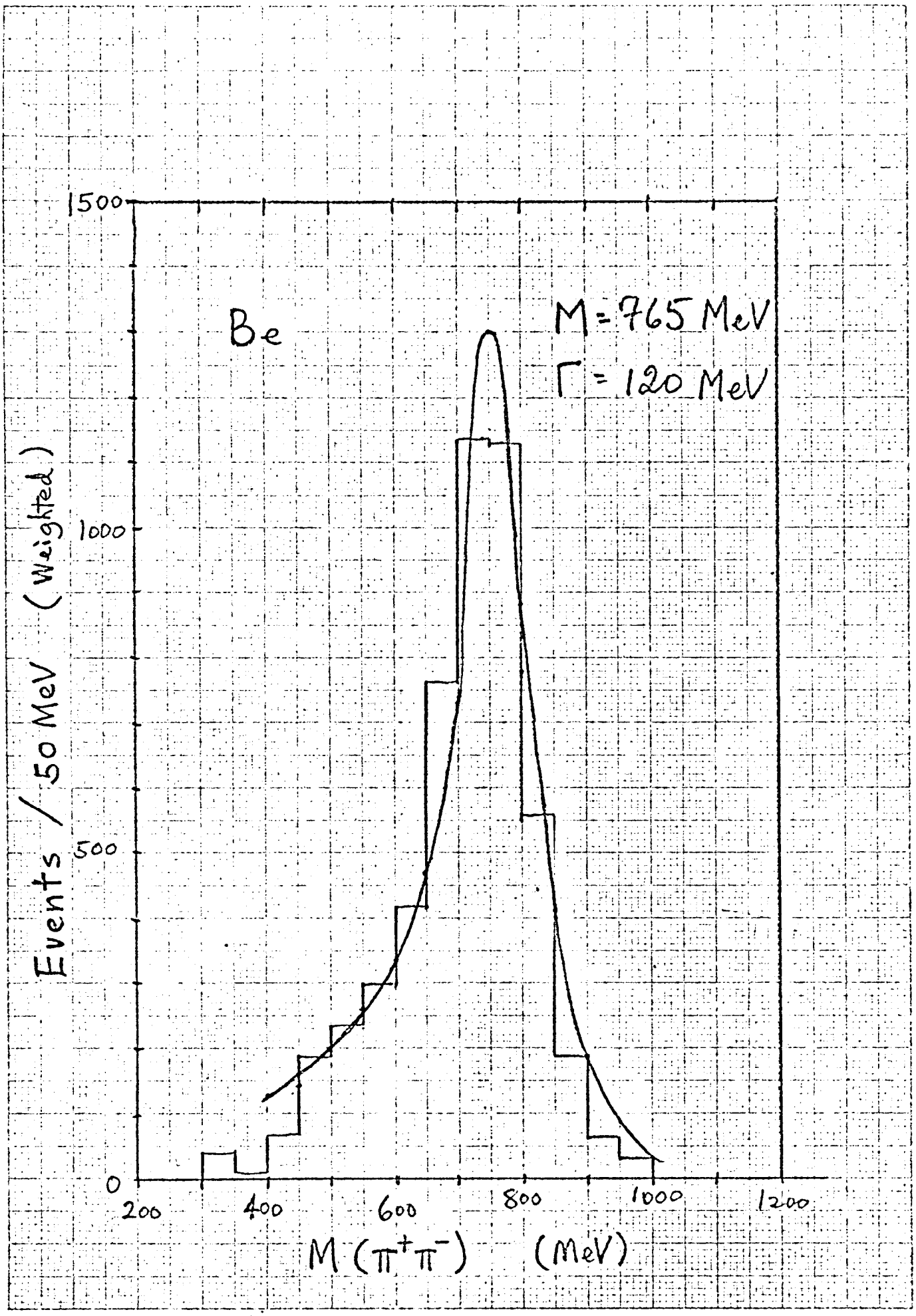
Be
M = 765 MeV
Γ = 120 MeV
Events / 50 MeV (Weighted)
1500
1000
500
0
200
400
600
800
1000
1200
M (π⁺π⁻) (MeV)

Fig.4a

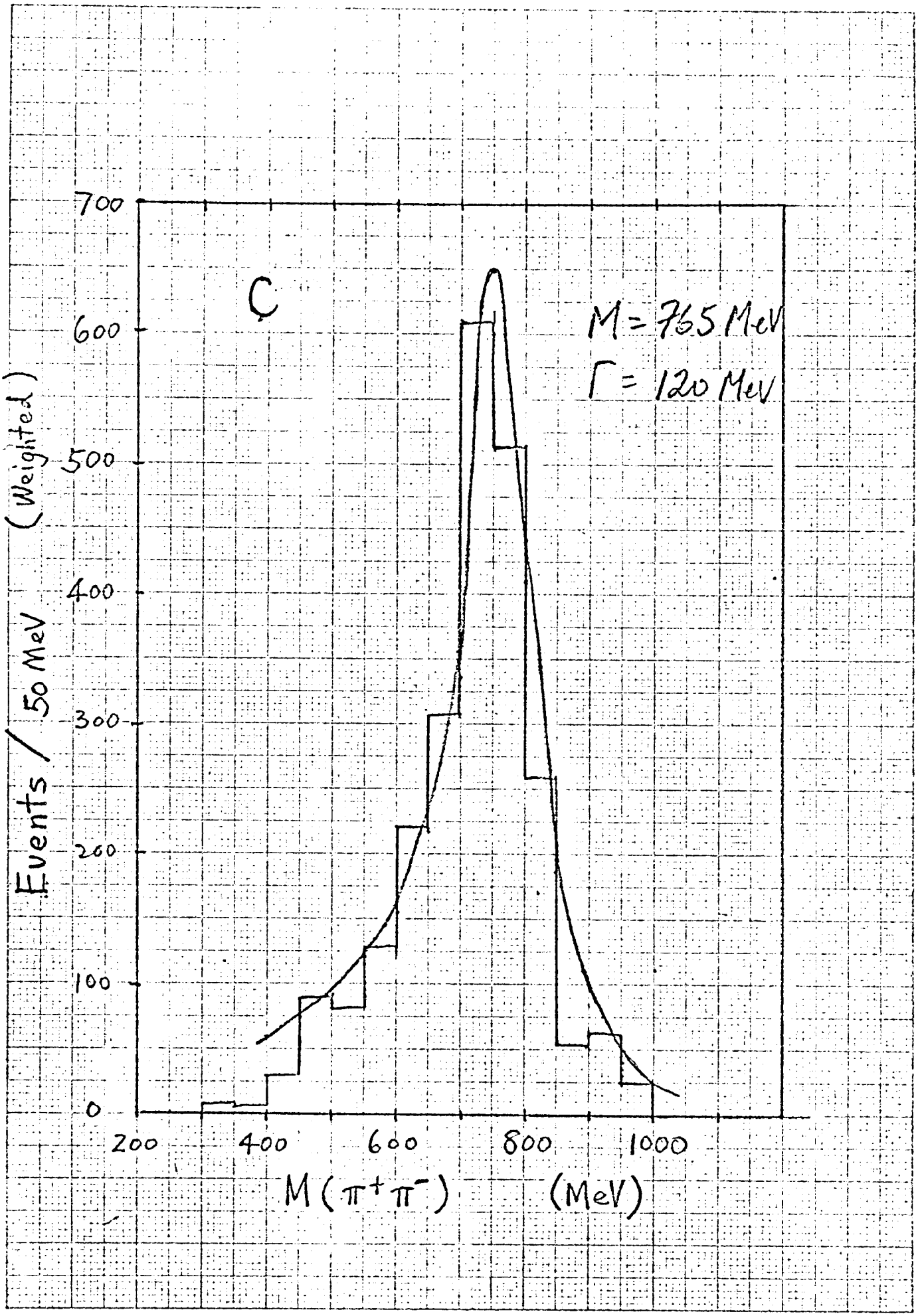
C
M = 765 MeV
Γ = 120 MeV
Events / 50 MeV (Weighted)
700
600
500
400
300
200
100
0
200
400
600
800
1000
M(π⁺π⁻) (MeV)

Fig.4t

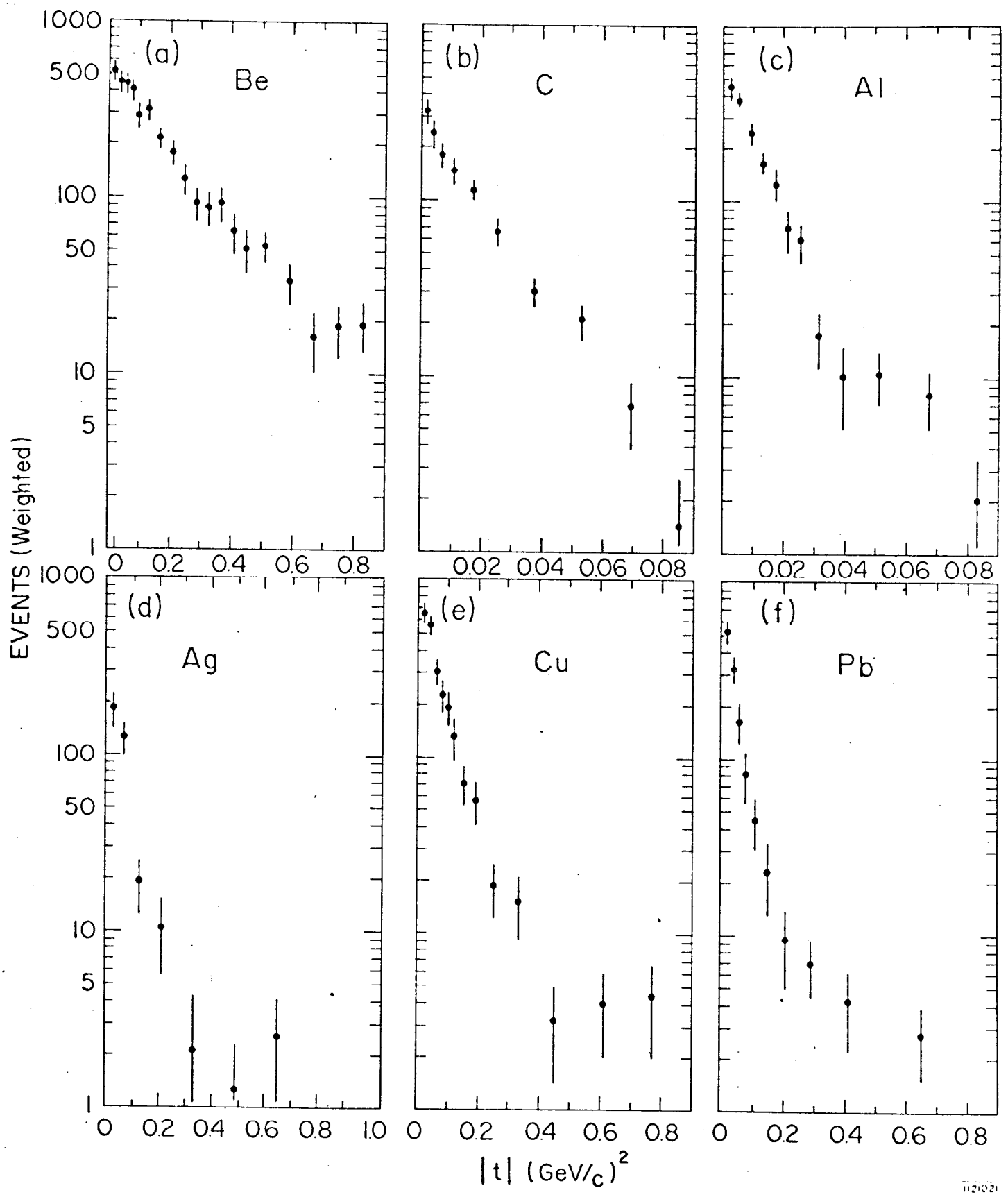
(a) Be
(b) C
(c) Al
(d) Ag
(e) Cu
(f) Pb
EVENTS (Weighted)
|t| (GeV/c)²
1000
500
100
50
10
5
1
0 0.2 0.4 0.6 0.8
0.02 0.04 0.06 0.08
0 0.2 0.4 0.6 0.8 1.0
1121021

Fig.5

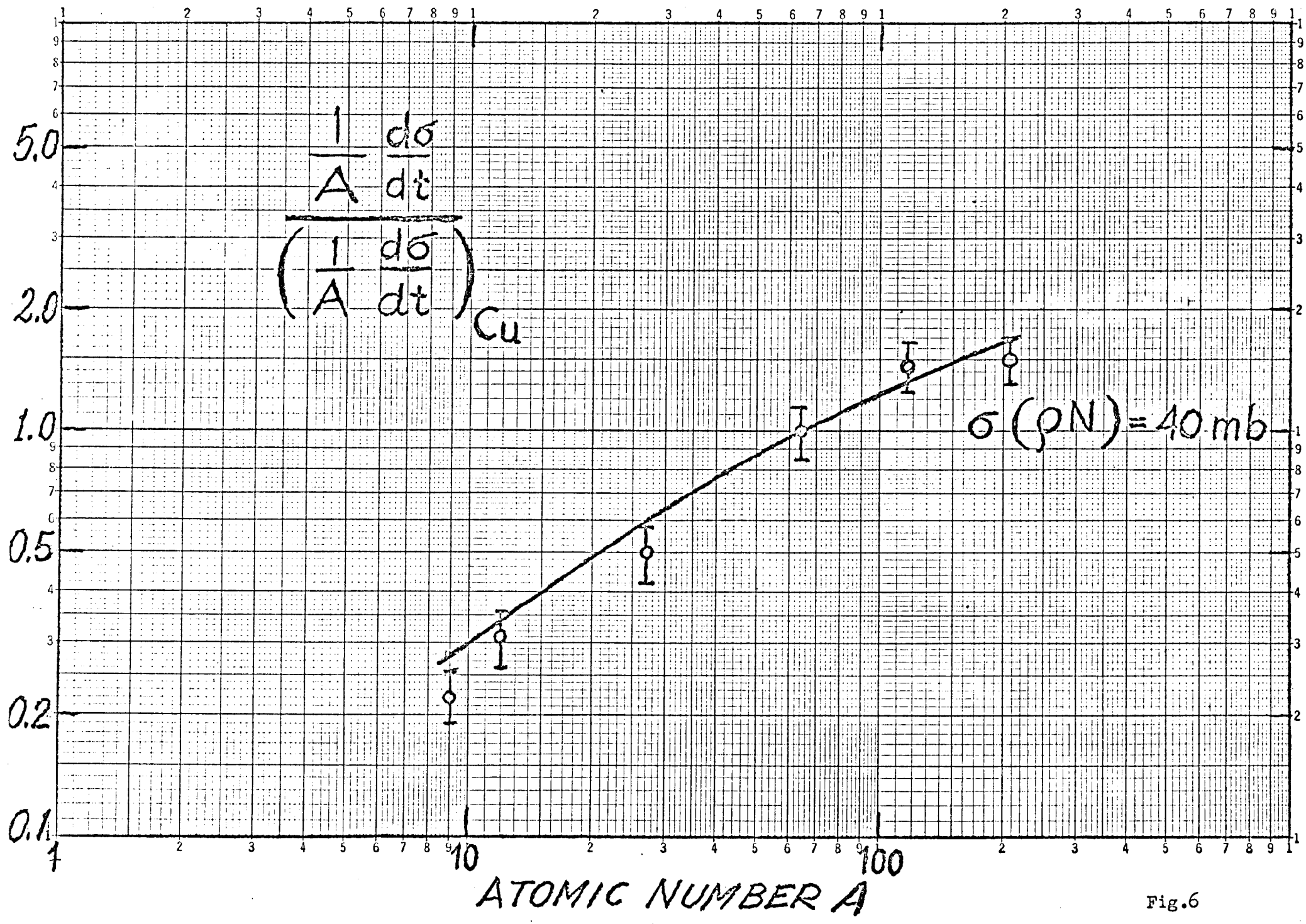
$\frac{\frac{1}{A}\frac{d\sigma}{dt}}{\left(\frac{1}{A}\frac{d\sigma}{dt}\right)_{Cu}}$
5.0
2.0
1.0
0.5
0.2
0.1
1
10
100
$\sigma(\rho N) = 40\,mb$
ATOMIC NUMBER A

Fig.6

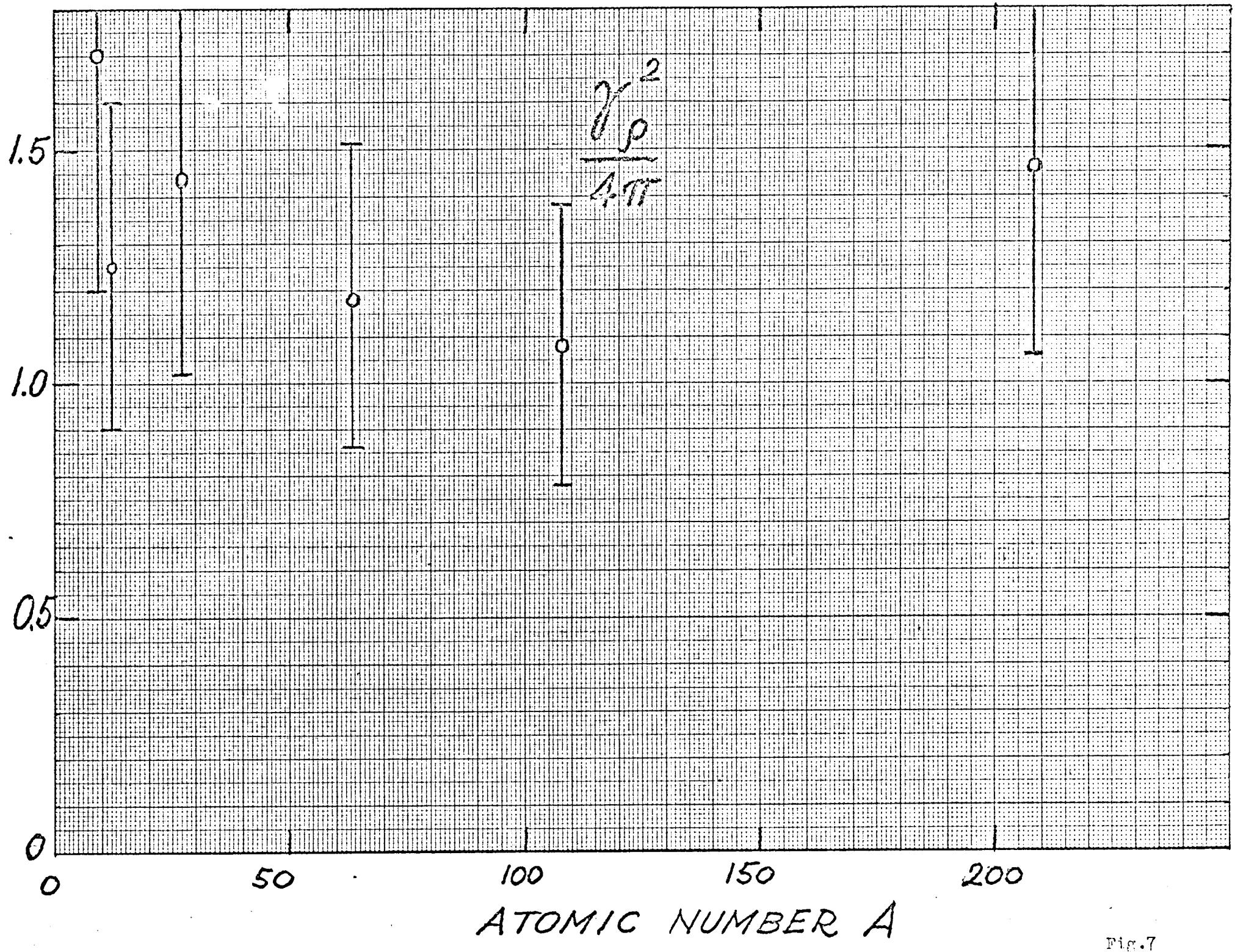

Fig.7

CORRECTIONS TO RAW DATA

Correction	Be	C	Al	Cu	Ag	Pb
1. Interactions in target	.90	.92	.95	.98	.99	.99
2. Mass section cut	.8	.8	.8	.8	.8	.8
3. Photon absorption in target	.96	.94	.92	.92	.92	.88
4. Pion decays in flight	.95	.95	.95	.95	.95	.95
5. Photon energy selection cut	.81	.81	.81	.84	.85	.81
6. Decay angle acceptance	.94	.94	.94	.94	.94	.94
Total Correction	.50 $\pm$ .13	.50 $\pm$ .13	.51 $\pm$.14	.54 $\pm$.15	.55 $\pm$.15	.51 $\pm$.14

p-p SCATTERING DIFFRACTION SLOPES

Material	A $(GeV/c)^{-2}$	R (Fermi)
Li	- 74	$3.4 \pm .1$
Be^{9}	- 77	$3.5 \pm .2$
C^{12}	- 67	$3.2 \pm .1$
Al^{27}	- 111	$4.2 \pm .1$
Cu^{64}	(200)	$5.6 \pm .1$
Pb^{207}	(362)	$7.5 \pm .3$
U^{238}	(362)	$7.5 \pm .4$

$$\frac{d\sigma}{dt} = \left.\frac{d\sigma}{dt}\right|_{o} e^{At}$$

$$A = \frac{R^2}{4\hbar^2}$$

ABSORPTION CROSS SECTIONS FOR p, $\pi^{\pm}$ IN COMPLEX NUCLEI

10.8 BeV/c

Particle / Material	π^+ (mb)	π^- (mb)	p (mb)
Carbon	213 ± 11	209 ± 11	254 ± 13
Aluminum	379 ± 20	374 ± 22	435 ± 23
Copper	704 ± 39	699 ± 41	775 ± 41
Tin	1091 ± 84	1075 ± 91	1058 ± 76
Lead	1650 ± 130	1670 ± 170	1490 ± 120

BNL 11598 W. Galbraith et al.

$$\frac{\gamma\rho^2}{4\pi} = \frac{\alpha}{64\pi} \cdot \frac{\sigma_\tau^2}{\left.\frac{d\sigma}{dt}\right|_{t=0}} \cdot \frac{1}{\hbar^2}$$

$$= 0.935 \times 10^2 \frac{\sigma_\tau^2}{\left.\frac{d\sigma}{dt}\right|_{t=0}}$$

(Where σ_τ is 10^{-24} cm^2

$\frac{d\sigma}{dt}$ is 10^{-27} cm^2/GeV^2).